

Low-Frequency Vibrations of Soft Colloidal Glasses

Ke Chen,¹ Wouter G. Ellenbroek,¹ Zexin Zhang,^{1,2} Daniel T.N. Chen,¹ Peter J. Yunker,¹ Silke Henkes,³ Carolina Brito,^{3,4} Olivier Dauchot,⁵ Wim van Saarloos,³ Andrea J. Liu,¹ and A. G. Yodh¹

¹*Department of Physics and Astronomy, University of Pennsylvania, Philadelphia, Pennsylvania 19104, USA*

²*Complex Assemblies of Soft Matter, CNRS-Rhodia-UPenn UMI 3254, Bristol, Pennsylvania 19007, USA*

³*Instituut-Lorentz, Universiteit Leiden, Postbus 9506, 2300 RA Leiden, The Netherlands*

⁴*Inst. de Física, Universidade Federal do Rio Grande do Sul, CP 15051, 91501-970, Porto Alegre RS, Brazil*

⁵*Service de Physique de l'État Condensé, CEA-Saclay; URA 2464, CNRS, 91191 Gif-sur-Yvette, France*

(Received 15 March 2010; published 9 July 2010)

We conduct experiments on two-dimensional packings of colloidal thermosensitive hydrogel particles whose packing fraction can be tuned above the jamming transition by varying the temperature. By measuring displacement correlations between particles, we extract the vibrational properties of a corresponding “shadow” system with the same configuration and interactions, but for which the dynamics of the particles are undamped. The vibrational properties are very similar to those predicted for zero-temperature sphere packings and found in atomic and molecular glasses; there is a boson peak at low frequency that shifts to higher frequency as the system is compressed above the jamming transition.

DOI: 10.1103/PhysRevLett.105.025501

PACS numbers: 63.50.Lm, 82.70.Dd

Crystalline solids are all alike in their vibrational properties at low frequencies; every disordered solid is disordered in its own way. Disordered solids nonetheless exhibit common low-frequency vibrational properties. Unlike crystals, which are dominated by sound modes, disordered solids generically exhibit a “boson peak,” where many more modes appear than expected for sound [1]. The excess modes of the boson peak are believed to be responsible for the unusual behavior of the heat capacity and thermal conductivity at low-to-intermediate temperatures in glasses [1,2].

A zero-temperature jamming transition may provide a framework for understanding this unexpected commonality [3]. For frictionless, idealized spheres this jamming transition lies at the threshold of mechanical stability, known as the isostatic point [3,4]. As a result of this coincidence, the vibrational behavior of the marginally jammed solid at densities just above the jamming transition is fundamentally different from that of ordinary elastic solids [5–8]. A new class of low-frequency vibrational modes arises because the system is at the threshold of mechanical stability [9]; these modes give rise to a divergent boson peak at zero frequency [5]. As the system is compressed beyond the jamming transition, the boson peak shrinks in height and shifts upwards in frequency [5], similar to what is seen in silica [10] and in polymer glasses [11]. Generalizations of the idealized sphere model suggest that the boson peaks of atomic or molecular glasses may be ascribed to the jamming transition [9,12–14].

Colloidal glasses offer signal advantages over atomic or molecular glasses because colloids can be tracked by video microscopy. Vibrational behavior has been explored in hard-sphere colloids [15] and vibrated granular packings [16]. Here we use deformable, thermosensitive hydrogel

particles to tune the packing fraction *in situ*. Our experiments show unambiguously that the commonality in vibrational properties observed in atomic and molecular glasses extends to colloidal glasses, in striking confirmation of the jamming scenario.

We study disordered colloidal solids of poly(*N*-isopropylacrylamide) or NIPA microgel particles. NIPA particles swell with decreasing temperature, and can thus be tuned at fixed number density from a loose packing of small particles to a jammed packing of deformed, larger particles over a temperature range of a few degrees. Particles were loaded between two glass cover slips, creating a monolayer in which the spheres were confined to move in the horizontal plane. A binary mixture (diameters 1 μm and 1.4 μm at $T = 24.7^\circ\text{C}$, with a large/small number ratio ~ 0.7) was employed to suppress crystallization. From separate brightness calibration studies, we estimate that the typical contact angle between small particles is within 13° from horizontal [17]. The sample was hermetically sealed using optical glue (Norland 63), and annealed for 2 h at 28°C . Data were acquired using standard bright field video microscopy at temperatures ranging from 24.7 to 27.2°C . Over this range the thermal energy is essentially constant, so that temperature serves primarily to change packing fraction. The temperature was controlled by thermal coupling to the microscope objective (BiOptechs), and the sample equilibrated for 15 min at each temperature before data acquisition over an area far from any boundaries or nonuniform regions within the sample. The trajectories of the $N \approx 3600$ particles in the field of view were extracted from videos at 30 frames/s using standard particle tracking techniques. No cage rearrangements occurred during the 1000 s of each run. Thus, the system remained in the same basin of the energy landscape.

Following [15], we define $\mathbf{u}(t)$ as the $2N$ -component vector of displacements of all particles from their average positions, and extract the time-averaged displacement correlation matrix (covariance matrix) [15,16,18]:

$$C_{ij} = \langle u_i(t)u_j(t) \rangle, \quad (1)$$

where $i, j = 1, \dots, 2N$ run over particles and coordinate directions, and the average runs over time frames.

In the harmonic approximation, the displacement correlations C are directly related to the stiffness matrix K , defined as the matrix of second derivatives of the effective pair interaction potential with respect to particle displacements. To quadratic order, the effective potential energy of the system is $V = \frac{1}{2}\mathbf{u}^T K \mathbf{u}$. Within the energy basin the system is thermally equilibrated, so we can calculate correlation functions from the partition function, $Z \propto \int D\mathbf{u} \exp(-\frac{1}{2}\beta\mathbf{u}^T K \mathbf{u})$, where $\beta = 1/k_B T$. In particular, $\langle u_i u_j \rangle = k_B T (K^{-1})_{ij}$.

We now introduce a shadow system of particles equilibrated in the same configuration with the same interactions as the colloids. In contrast to the colloids, which are suspended in water and whose motion is strongly damped, the virtual particles of the shadow system are undamped. The real and shadow systems are characterized by the same correlation and stiffness matrices, C and K , because these are static equilibrium quantities. For the shadow system, however, the stiffness matrix is directly related to the dynamical matrix

$$D_{ij} = \frac{K_{ij}}{m_i} = \frac{k_B T (C^{-1})_{ij}}{m_i} \quad (2)$$

whose eigenvectors correspond to the vibrational modes. Thus, this analysis [15] allows direct comparison of the damped colloidal solid to disordered atomic or molecular glasses and to idealized sphere packings.

One advantage of this analysis is that vibrational information can be obtained without knowing the effective interaction potential between particles. As an added bonus, we can extract information about the interactions. The elements of stiffness matrix K contain direct information about the second derivative of the effective pair potential, denoted as k_{ij} . We find that k_{ij} is far above the noise only for adjacent particles. This observation gives us confidence in the method; clearly, elastic interactions between neighboring particles dominate the data, as they should. The particle separations are known sufficiently accurately for large-large pairs [17]; we therefore obtain $k(r)$. We fit $k(r)$ to the second derivative of the harmonic ($\alpha = 2$) or 3D Hertzian ($\alpha = 5/2$) potentials:

$$V(r_{ij}) = \frac{\epsilon}{\alpha} \left(1 - \frac{r_{ij}}{R_i + R_j} \right)^\alpha \quad r_{ij} \leq R_i + R_j, \quad (3)$$

and $V = 0$ otherwise, where R_i is the radius of particle i . We convolute the fitting functions with a Gaussian distribution to account for the known colloidal particle polydispersity. The results are plotted in Fig. 1. Note that we

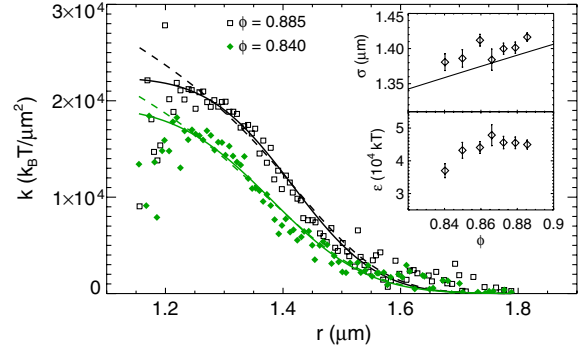


FIG. 1 (color online). The effective spring constant k_{ij} between large particles, extracted from the stiffness matrix K at $\phi = 0.885$ (squares), and $\phi = 0.840$ (diamonds). The results are fit to harmonic (solid), and Hertzian (dashed) repulsions, convoluted with the particle size distribution. Insets: Fitted interaction range σ and energy ϵ for the harmonic case as a function of ϕ . Solid line in upper inset: the particle diameter implied by the packing fraction.

cannot differentiate between the harmonic and Hertzian fits; they differ only at large overlaps where statistics are limited. The fit parameters ϵ and $\sigma = \langle R_i + R_j \rangle$ for the harmonic potential are shown as insets in Fig. 1. As expected, σ increases with ϕ and ϵ is roughly constant for $\phi > 0.84$. The solid curve in the top inset of Fig. 1 shows the value of the diameter implicit in the assignment of ϕ obtained by interpolation of dynamic light scattering data at different temperatures at low concentration. Here we have measured the elastic contact distance while dynamic light scattering measures a hydrodynamic radius. The uncertainty in the solid curve is larger than the difference between the curve and our data. The correlation method therefore provides a new way of measuring interparticle interactions at high concentrations.

The accuracy of our results depends on the ability to resolve particle displacements $\mathbf{u}(t)$ as well as the statistics of the time averages in Eq. (1). The optical resolution, $\epsilon \approx 5$ nm, at best in our case, must be small compared to the average root-mean-squared displacement, calculated to be $c = \langle C_{ii}^{1/2} \rangle \approx 22$ nm at the packing fraction $\phi = 0.859$. Likewise, the number of degrees of freedom, $2N \approx 7200$, should be small compared to the number of time frames over which C_{ij} is averaged, $T = 30000$, at most in our case. Figures 2(a) and 2(b) show the density of vibrational states relative to the Debye prediction, $D(\omega)/\omega$, as ϵ/c and $2N/T$ are varied. $D(\omega)$ is normalized so that $\int_0^\infty D(\omega) d\omega = 2N$, and ϵ is varied by rounding measured particle displacements. Poor resolution artificially lowers the high end of the spectrum but inadequate statistics raise the high end, so that the two effects tend to cancel. The spectrum appears close to convergence for the standard values $T = 30000$ and $\epsilon = 5$ nm. The error in the spectrum width for these values is estimated as 10% [16,19]. We also reduced the sample area studied and found negligible dependence on sample size [17].

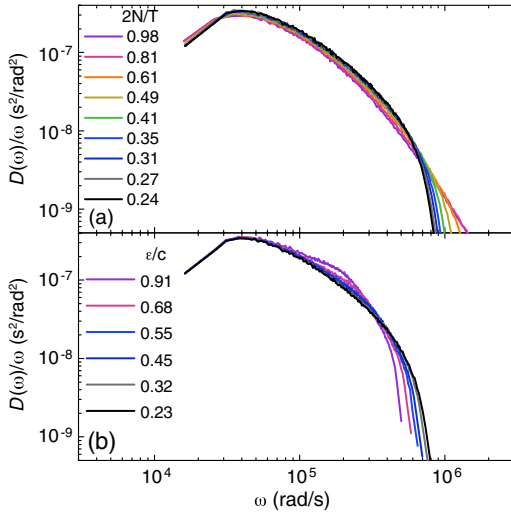


FIG. 2 (color online). $D(\omega)/\omega$ at $\phi = 0.859$ averaged over (a) different ratios $2N/T$ of the number of degrees of freedom to the number of frames, and (b) different values of the optical resolution relative to the average rms displacement, ϵ/c .

The vibrational spectrum for two-dimensional crystals has the Debye form, $D(\omega) \sim \omega$. In Fig. 3(a) we plot the measured density of states relative to the Debye prediction, $D(\omega)/\omega$, at $\phi = 0.859$, well above the jamming transition at $\phi_c \approx 0.84$ [20] [21]. For an elastic solid such as a crystal, $D(\omega)/\omega$ would be flat at low frequencies; the presence of a maximum in Fig. 3(a) indicates the existence

of a boson peak and the position of the maximum defines the boson peak frequency, ω^* . Thus Fig. 3(a) shows that a boson peak—an important feature in the vibrational spectrum of atomic and molecular glasses—also appears in a disordered colloidal solid.

Figure 3(c) shows the participation ratio, $p(\omega)$, which measures the degree of spatial localization of a mode n : $p(\omega_n) = (\sum_i m_i |\mathbf{e}_{n,i}|^2)^2 / (N \sum_i m_i^2 |\mathbf{e}_{n,i}|^4)$, where $\mathbf{e}_{n,i}$ is the polarization vector in mode n and m_i is the mass, of particle i . Thus, $p(\omega_n) \sim 1/N$ for a localized mode and $p(\omega_n) \sim \mathcal{O}(1)$ for an extended mode. The results are qualitatively the same if we do not weight the sums with the particle masses.

At low frequency, Fig. 3(c) shows that the modes are clearly very different from plane-wave sound modes because they have a low participation ratio; Fig. 3(d) depicts a typical low-frequency mode. It is quasilocalized with localized structure superimposed on a plane-wave-like background. At intermediate frequencies, eigenmodes are highly disordered and extended with $p \sim \mathcal{O}(1)$ [Fig. 3(e)] while at high frequencies the modes are localized, as expected [Fig. 3(f)].

Figure 4(a) shows $D(\omega)/\omega$ as a function of packing fraction ϕ . As expected, the boson peak shrinks and shifts up in frequency with ϕ [5]. For athermal frictionless spheres with Eq. (3), the inverse boson peak height and frequency scale as $(\phi - \phi_c)^{(\alpha-1)(d/2)-1/2}$ and $(\phi - \phi_c)^{(\alpha-1)/2}$, respectively, in d dimensions. For $d = \alpha = 2$ the two scalings are the same, and for $\alpha = 5/2$ they are

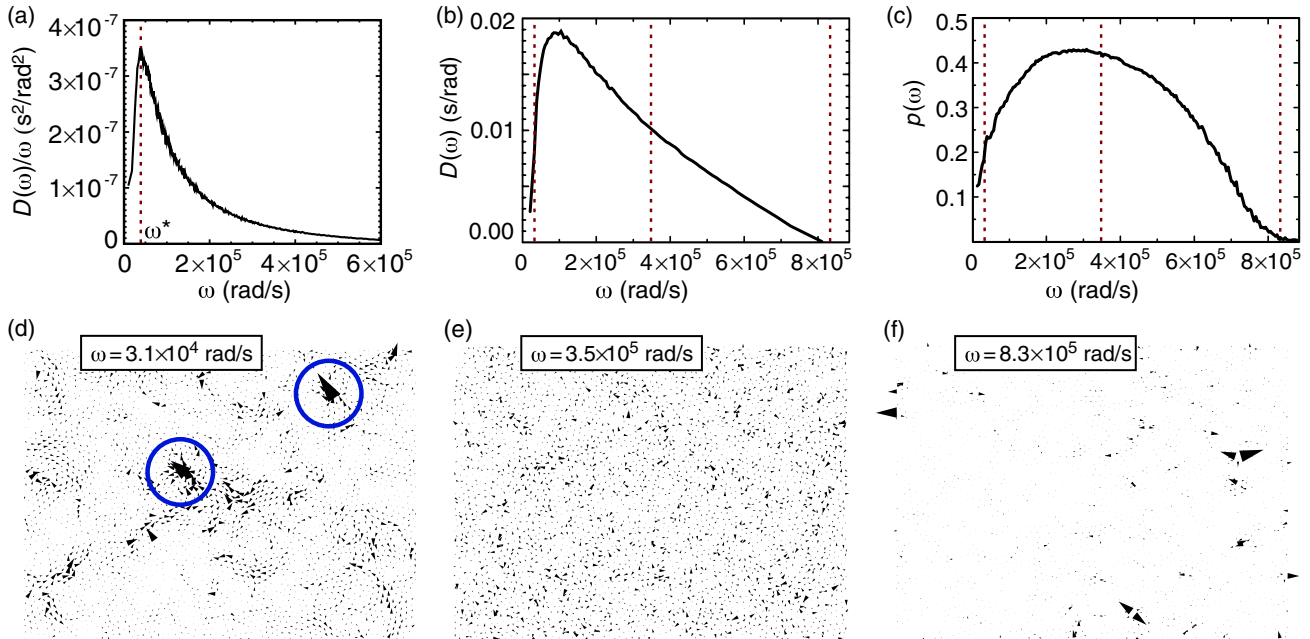


FIG. 3 (color online). (a) The vibrational density of states relative to the Debye prediction, $D(\omega)/\omega$, for $\phi = 0.859$. The maximum in this plot, shown by the vertical dashed line, defines the boson peak frequency, ω^* . (b) $D(\omega)$, and (c) the participation ratio $p(\omega)$. The dotted vertical lines in (b) and (c) indicate the frequencies of the modes shown in the remaining panels. (d)–(f) Eigenmodes at (d) low, (e) intermediate, and (f) high ω . The size of each arrow scales with the displacement of the particle there, weighted by its mass: $|\mathbf{u}_i|/\sqrt{m_i}$. Blue circles in (d) indicate high-displacement regions.

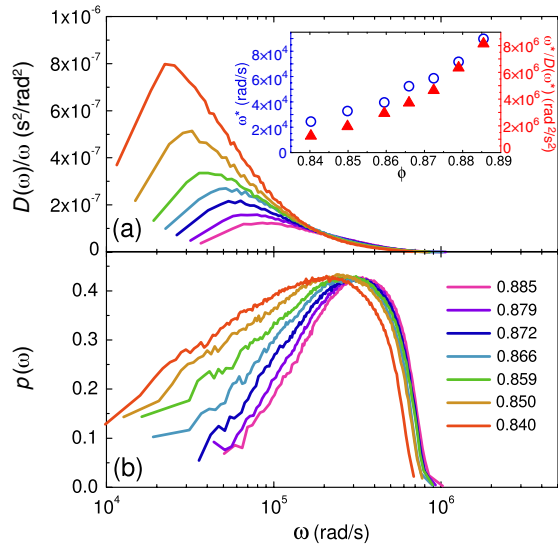


FIG. 4 (color online). (a) $D(\omega)/\omega$ and (b) participation ratio vs ω as a function of packing fraction [as labeled in (b)]. Inset to (a): the boson peak frequency ω^* (circles, left) and inverse peak height $\omega^*/D(\omega^*)$ (triangles, right) vs ϕ .

very close. Consistent with this, the inset to Fig. 4(a) shows very similar ϕ dependence for the two quantities. In fact, the curves collapse upon rescaling accordingly [17]. In $d = 2$ this also predicts that $D(\omega^*)/\omega^* \sim G^{-1}$, where G is the shear modulus [17,23]. Note, however, that it is difficult to extract scaling exponents because thermal effects smooth the jamming transition around ϕ_c [24].

Figure 4(b) shows that the shape of $p(\omega)$ is similar at all packing fractions. As the system is decompressed towards ϕ_c , however, the low- ω quasilocalized modes shift down in frequency, edging closer to instability [8].

By examining displacement correlations in a 2D colloidal glass, we studied its vibrational properties without *a priori* knowledge of the particle interactions. A boson peak that grows and shifts to lower frequency as the packing fraction decreases towards unjamming was found, and quasilocalized modes below the boson peak were identified. Similar quasilocalized modes have been observed in idealized spheres as well as in atomic or molecular glasses (see [8] and references therein). In sphere packings, these modes are associated with the lowest energy barriers for rearrangements [8]. Under mechanical load, such a mode shifts to zero frequency, signaling a rearrangement [25] that occurs where the mode has high displacements [circled in Fig. 3(d)] [26]. Thermally driven irreversible particle rearrangements, observed in aging glasses [27], are also connected to low-frequency quasilocalized modes [28]. Thus, our experiments demonstrate that it is possible to identify localized regions that are predisposed towards rearrangements.

We thank N. Xu, D. Bonn, J. Crocker, D. J. Durian, and S. R. Nagel for helpful discussions. This work was funded by DMR 0804881 (A. G. Y.), PENN-MRSEC DMR-0520020 (K. C. and W. G. E.), NASA NNX08AO0G (A. G. Y.), and DOE DE-FG02-05ER46199 (A. J. L. and W. G. E.).

- [1] *Amorphous Solids*, edited by W. A. Phillips (Springer-Verlag, Berlin, 1981).
- [2] R. O. Pohl, X. Liu, and E. Thompson, *Rev. Mod. Phys.* **74**, 991 (2002).
- [3] A. J. Liu and S. Nagel, *Ann. Rev. Condens. Matter Phys.* (to be published).
- [4] C. S. O'Hern *et al.*, *Phys. Rev. E* **68**, 011306 (2003).
- [5] L. E. Silbert, A. J. Liu, and S. R. Nagel, *Phys. Rev. Lett.* **95**, 098301 (2005).
- [6] M. Wyart, S. R. Nagel, and T. A. Witten, *Europhys. Lett.* **72**, 486 (2005).
- [7] N. Xu *et al.*, *Phys. Rev. Lett.* **102**, 038001 (2009).
- [8] N. Xu *et al.*, *Europhys. Lett.* **90**, 56001 (2010).
- [9] M. Wyart, *Ann. Phys. (Paris)* **30**, 1 (2005).
- [10] S. Sugai and A. Onodera, *Phys. Rev. Lett.* **77**, 4210 (1996); Y. Inamura *et al.*, *Physica (Amsterdam)* **284B-288B**, 1157 (2000); K. Trachenko *et al.*, *Phys. Rev. Lett.* **93**, 135502 (2004).
- [11] L. Hong *et al.*, *Phys. Rev. B* **78**, 134201 (2008).
- [12] N. Xu *et al.*, *Phys. Rev. Lett.* **98**, 175502 (2007).
- [13] M. Wyart *et al.*, *Phys. Rev. Lett.* **101**, 215501 (2008).
- [14] M. Wyart, in *Rigidity and Boolchand Intermediate Phases in Nanomaterials*, edited by M. Micoulaut and M. Popescu (INOE, Bucharest, 2009).
- [15] A. Ghosh *et al.*, *Phys. Rev. Lett.* **104**, 248305 (2010).
- [16] C. Brito *et al.*, *Soft Matter* **6**, 3013 (2010).
- [17] See supplementary material at <http://link.aps.org/supplemental/10.1103/PhysRevLett.105.025501> for additional experimental details.
- [18] D. Kaya *et al.*, <http://meetings.aps.org/link/BAPS.2010.MAR.D12.2>.
- [19] S. Henkes *et al.* (unpublished).
- [20] Z. Zhang *et al.*, *Nature (London)* **459**, 230 (2009).
- [21] We define $\phi_c \approx 0.84$ as the onset of jamming for this system following earlier experiments on the same system [20]. At this packing fraction, the peak in the dynamic susceptibility, χ_4 , passes out of our time window, and the first peak of the pair correlation function $g(r)$ exhibits a maximum [20].
- [22] L. E. Silbert, A. J. Liu, and S. R. Nagel, *Phys. Rev. E* **79**, 021308 (2009).
- [23] H. Shintani and H. Tanaka, *Nature Mater.* **7**, 870 (2008).
- [24] N. Xu, [arXiv:0911.1576](https://arxiv.org/abs/0911.1576).
- [25] C. E. Maloney and A. Lemaître, *Phys. Rev. E* **74**, 016118 (2006).
- [26] M. E. Manning and A. J. Liu (private communication).
- [27] P. Yunker *et al.*, *Phys. Rev. Lett.* **103**, 115701 (2009).
- [28] A. Widmer-Cooper *et al.*, *Nature Phys.* **4**, 711 (2008); *J. Chem. Phys.* **131**, 194508 (2009); C. Brito and M. Wyart, *J. Stat. Mech.* **08** (2007) L08003.